
Interpolation Technique to Speed Up Gradients Propagation in Neural ODEs

Talgat Daulbaev, Alexandr Katrutsa, Larisa Markeeva, Julia Gusak,
Andrzej Cichocki, Ivan Oseledets
Skolkovo Institute of Science and Technology
Moscow, Russia
talgat.daulbaev@skoltech.ru
aleksandr.katrutsa@phystech.edu
{l.markeeva,y.gusak,a.cichocki,i.oseledets}@skoltech.ru

Abstract

We propose a simple interpolation-based method for the efficient approximation of gradients in neural ODE models. We compare it with the reverse dynamic method (known in the literature as “adjoint method”) to train neural ODEs on classification, density estimation, and inference approximation tasks. We also propose a theoretical justification of our approach using logarithmic norm formalism. As a result, our method allows faster model training than the reverse dynamic method that was confirmed and validated by extensive numerical experiments for several standard benchmarks.

1 Introduction

We propose a novel method to train neural ordinary differential equations (neural ODEs) [1]. This method performs stable and memory-efficient backpropagation through the solution of initial value problems (IVP). Throughout the study, we use the term neural ODEs for all neural networks with so-called ODE blocks. An ODE block is a continuous analog of a residual neural network [2] that can be considered as Euler discretization of ordinary differential equations. Neural ODEs have already been successfully applied to various machine learning problems, including classification, generative modeling, and time series prediction [1, 3, 4].

ODE block is a neural network layer that takes the activations z_0 from the previous layer as input, solves the initial value problem (IVP) described as

$$\begin{cases} \frac{dz}{dt} = f(z(t), t, \theta), & t \in [t_0, t_1] \\ z(t_0) = z_0, \end{cases} \quad (1)$$

and solved by any ODE solver. Note, the right-hand side in IVP (1) depends on set of parameters θ which is gradually updated during training. Therefore, during the backward pass in neural ODEs, the loss function L , which depends on the solution of the IVP, should be differentiated with respect to parameter θ . A direct application of backpropagation to ODE solvers require a huge memory, since for every time step τ_k , the output $z(\tau_k)$ must be stored as a part of the computational graph.

However, the approach based on the *adjoint method* [5, 6] helps to propagate gradients through the initial value problem with a relatively small memory footprint. Originally adjoint method has been actively used in mathematical modeling, for example, in seismograph and climate studies [7, 8]. It was used to investigate the sensitivity of the model output with respect to the input. In the context of training neural ODEs, the adjoint method is modified to combine it with the standard backpropagation [1]. We refer to this modified adjoint method as *reverse dynamic method* (RDM).

This method yields solving the augmented initial value problem backward-in-time. We call this IVP as the *adjoint IVP*. One of the components of the adjoint IVP is IVP that defines $z(t), t \in [0, 1]$. Therefore, the numerical solving of the adjoint IVP does not require storing intermediate activations $z(\tau_k)$ during the forward pass. As a result, the memory footprint becomes smaller.

However, Gholami et al. [9] showed that the RDM might lead to catastrophic numerical instabilities. To address this issue, the authors introduce a method called ANODE. This method exploits *checkpointing* idea [10], i.e., propose to store checkpoints $z(\tau_k)$ at intermediate selected time points τ_k during the forward pass. As result of this, in the backward pass, ANODE performs additional ODE solver steps forward-in-time in each interval between sequential checkpoints. The intermediate activations are stored to compute the target gradient. The main disadvantage of ANODE is that it requires intermediate activations storage and need to perform additional ODE solver steps.

To address the instability of the reverse dynamic method and limitations of ANODE, we propose *interpolated reverse dynamic method* (IRDM), which is described in detail in Section 2. This method is based on a smooth function interpolation technique to approximate $z(t)$ and exclude the IVP that defines $z(t)$ from the adjoint IVP. Thus, we do not reverse IVP (1) and avoid the instability problem of the reverse dynamic method. Under mild conditions on the right-hand side $f(z(t), t, \theta)$, function $z(t)$ is continuously differentiable as a solution of IVP, i.e. $z(t) \in C^1[t_0, t_1]$. Therefore, it can be approximated with the *barycentric Lagrange interpolation* (BLI) [11] on a Chebyshev grid. This technique is widely used for interpolation problems [11]. To construct such approximation, one has to store activations $z(t)$ in the point from the Chebyshev grid during the forward pass. These activations can be computed with DOPRI5 adaptive ODE solver without additional right-hand side evaluations [12]. After that, in the backward pass, stored activations are used to approximate $z(t)$ during the adjoint IVP solving. The main requirement for our method to work correctly and efficiently is that $z(t)$ can be approximated by BLI with sufficient accuracy. This can only be verified experimentally. However, the accuracy of such approximation is inherently related to the smoothness of the solution, which is also one of the main motivations behind using neural ODEs.

Our main contributions are the following.

- We propose *interpolated reverse dynamic method* to train neural ODEs. This method uses approximated activations $z(t)$ in the backward pass and reduces the dimension of the initial value problem, that is used to compute the gradient. Thus, the training becomes faster.
- We present the error bound for the gradient norm under small perturbation of the activations $z(t)$ induced by using interpolated values.
- We have evaluated our approach on density estimation, inference approximation, and classification tasks and showed its effectiveness in terms of test loss-training time trade-off compared to the reverse dynamic method.

2 Interpolated Reverse Dynamic Method

Deep learning problems are usually solved by minimizing a loss function L with respect to model parameters using gradient-based methods. To compute the gradient $\frac{\partial L}{\partial \theta}$ without saving computational graph from the forward pass, the *adjoint method* can be used [13, 14].

Adjoint method. The main idea of the adjoint method is to derive gradients of the loss function L from the first-order optimality conditions (FOOC) for a constrained optimization problem. In our case, the optimization problem is formulated as the loss minimization with ODE constraint in the form of (1).

To construct the corresponding Lagrangian, the adjoint variable $\mathbf{a}(t)$ is introduced

$$\mathcal{L}(z(t), \theta, \mathbf{a}(t)) = L(z(t_1), \theta) + \int_{t_0}^{t_1} \mathbf{a}(t) \left(\frac{dz}{dt} - f(z(t), t, \theta) \right) dt,$$

and the FOOC can be written in the following form

$$\frac{\delta \mathcal{L}}{\delta \mathbf{a}(t)} = \mathbf{0} \rightarrow \frac{d\mathbf{z}}{dt} - f(\mathbf{z}(t), t, \boldsymbol{\theta}) = \mathbf{0} \quad (2)$$

$$\frac{\delta \mathcal{L}}{\delta \mathbf{z}(t)} = \mathbf{0} \rightarrow \begin{cases} \frac{d\mathbf{a}}{dt} = -\mathbf{a}(t)^\top \frac{\partial f(\mathbf{z}(t), t, \boldsymbol{\theta})}{\partial \mathbf{z}} \\ \mathbf{a}(t_1) - \frac{\partial L}{\partial \mathbf{z}(t_1)} = \mathbf{0} \end{cases} \quad (3)$$

$$\frac{\delta \mathcal{L}}{\delta \boldsymbol{\theta}} = \mathbf{0} \rightarrow \frac{\partial L}{\partial \boldsymbol{\theta}} = \int_{t_0}^{t_1} \mathbf{a}(t)^\top \frac{\partial f(\mathbf{z}(t), t, \boldsymbol{\theta})}{\partial \boldsymbol{\theta}} dt. \quad (4)$$

Hence, the target gradient $\frac{\partial L}{\partial \boldsymbol{\theta}}$ can be computed in the following way: ODE (2) gives the activation dynamic $\mathbf{z}(t)$, ODE (3) gives the adjoint variable $\mathbf{a}(t)$ based on $\mathbf{z}(t)$ and finally the target gradient $\frac{\partial L}{\partial \boldsymbol{\theta}}$ is computed with the integral in (4). The adjoint method assumes that activations $\mathbf{z}(t_0) = \mathbf{z}_0$ are known in the backward pass. Thus, IVP (1) is solved forward-in-time, IVP (3) is solved backward-in-time and integral (4) is computed based on the derived $\mathbf{a}(t)$ and $\mathbf{z}(t)$. The adjoint method requires storing gradients $\frac{\partial f}{\partial \boldsymbol{\theta}}$ and $\frac{\partial f}{\partial \mathbf{z}}$ in intermediate activations $\mathbf{z}(t), t \in [t_0, t_1]$. Therefore, to reduce its memory consumption, the checkpointing idea is used.

Checkpointing in the adjoint method. ANODE method [9] exploits checkpointing idea to get the target gradient $\frac{\partial L}{\partial \boldsymbol{\theta}}$. This method stores some intermediate activations $\mathbf{z}(t)$ in the forward pass. These activations are called checkpoints. In the backward pass, ANODE considers intervals between sequential checkpoints from the right side to the left side. In every interval, ODE (2) with an initial condition equal to the checkpoint on the left is solved forward-in-time, IVP (3) is solved backward-in-time and the integral is updated. This approach is illustrated in Figure 1d. This approach still requires additional memory to store checkpoints and gradients $\frac{\partial f}{\partial \boldsymbol{\theta}}$. Also, it solves ODE (2) with multiple initial conditions equal to checkpoints. These drawbacks are fixed in reverse dynamic method [1].

Reverse dynamic method. This method is used in [1], where the neural ODE model is proposed, under the name ‘‘adjoint method’’. The reverse dynamic method assumes that activations $\mathbf{z}(t_1) = \mathbf{z}_1$ are known and do not store any checkpoints during the backward pass. Therefore, in the backward pass, the following IVP is solved backward-in-time and defines activations:

$$\begin{cases} \frac{d\mathbf{z}}{dt} = f(\mathbf{z}(t), t, \boldsymbol{\theta}) \\ \mathbf{z}(t_1) = \mathbf{z}_1, \end{cases} \quad (5)$$

IVP (3) is solved backward-in-time and integral (4) is computed as the solution of the following IVP:

$$\begin{cases} \frac{d}{dt} \left(\frac{\partial L}{\partial \boldsymbol{\theta}} \right) = -\mathbf{a}(t)^\top \frac{\partial f(\mathbf{z}(t), t, \boldsymbol{\theta})}{\partial \boldsymbol{\theta}} \\ \frac{\partial L}{\partial \boldsymbol{\theta}}(t_1) = \mathbf{0}. \end{cases} \quad (6)$$

Thus, IVPs (3),(5) and (6) can be composed in the augmented IVP that is solved backward-in-time. This method is illustrated in Figure 1a. The study [9] demonstrates that this method can be unstable due to the reverse IVP (1). To get the right trade-off between stability and memory consumption, we propose *interpolated reverse dynamic method* (IRDM).

Interpolated reverse dynamic method. In the proposed *interpolated reverse dynamic method* (IRDM), we suggest to eliminate (5) from the adjoint IVP. Instead of using IVP (5) to get activations $\mathbf{z}(t)$, the IRDM approximates them through the barycentric Lagrange interpolation (BLI) on a Chebyshev grid [11]. This method is summarized in Figure 1c. We urge readers not to confuse the Lagrange interpolation, which is mostly of theoretical interest, with the BLI, that is widely used in practice for polynomial interpolation [15].

Denote by $\hat{\mathbf{z}}(t)$ the interpolated activations with the BLI technique that are used in the backward pass. As described in [15], $\hat{\mathbf{z}}(t)$ can be computed with the following equation:

$$\hat{\mathbf{z}}(t) = \left(\sum_{n=0}^N \frac{w_n}{t - \tau_n} \hat{\mathbf{z}}_n \right) / \left(\sum_{n=0}^N \frac{w_n}{t - \tau_n} \right), \quad (7)$$

where the sequence $\{\tau_n\}_{n=0}^N$ form the Chebyshev grid, and $t_0 = \tau_0 < \tau_1 < \dots < \tau_N = t_1$, $\hat{\mathbf{z}}_n \triangleq \mathbf{z}(\tau_n)$ are exact activations computed in the Chebyshev grid during the forward pass and stored

to be used in the backward pass. To get these activations during the forward pass, we explore features of DOPRI5 adaptive solver [12] to compute activations in given time points (e.g., in Chebyshev grid) without additional right-hand side evaluations. Thus, we store $z(\tau_n)$ and solve IVP (1) simultaneously. The weights w_n are computed as follows once for the entire training process

$$w_n = (-1)^n \sin\left(\frac{(2n+1)\pi}{2N+2}\right).$$

The computational complexity of computing $\hat{z}(t)$, as well as additional memory usage, is $O(N)$. Since we approximate $z(t)$, only (3) and (6) have to be solved backward-in-time during the backward pass. Thus, the dimension of the backward IVP is reduced by the size of the activations $z(t)$.

From the theory of polynomial interpolation, it is known, that if $z(t)$ is analytic function, then the following bound on the BLI approximation error holds

$$\max_{t \in [0,1]} \|\hat{z}(t) - z(t)\|_\infty \leq \mathcal{O}(M^{-N}), \quad (8)$$

where $M > 1$ depends on the region where the activation dynamic $z(t)$ is analytic, more details see in [15, 16, 17]. The solution of IVP (1) is analytic if the right-hand side $f(z(t), t, \theta)$ is analytic [18].

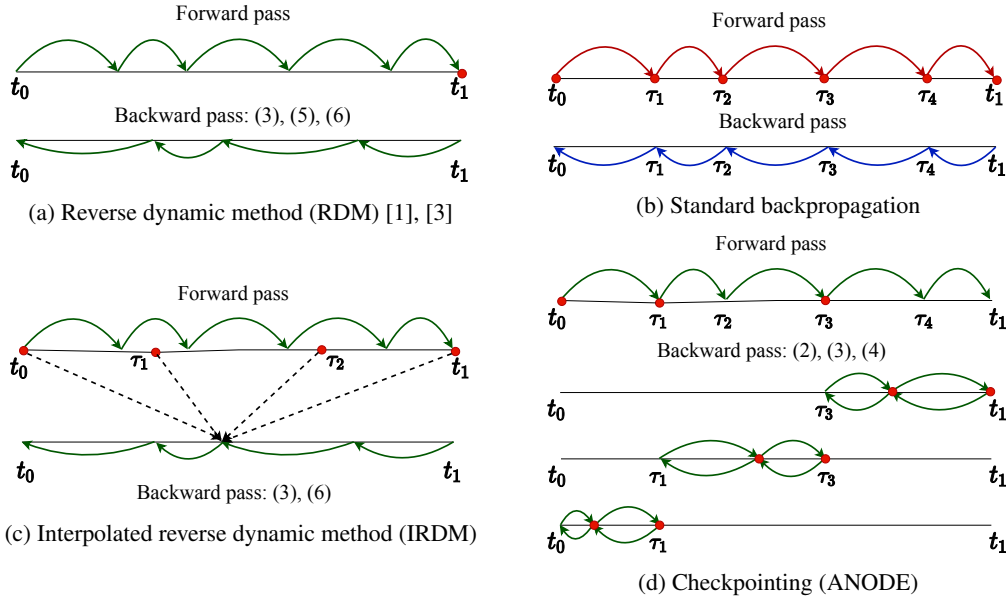


Figure 1: Comparison of different schemes to make forward and backward passes through the ODE block. Red circles indicate that the activations are stored at these time points. Red arrows indicate that during ODE steps, the outputs of the intermediate layer are stored to propagate gradients. Green arrows correspond to the steps with ODE solvers. Blue arrows correspond to the steps with automatic differentiation through the stored computational graph. Activations in Chebyshev grid points (t_0, τ_1, τ_2 and t_1 in Figure 1c) are stored in the interpolation approach during the forward pass. Chebyshev grid points do not necessarily coincide with time steps of ODE solver, but activations in these points can be recovered from the computed activations with ODE solver. The stored activations are used to approximate activations in the backward pass. The dotted arrows in Figure 1c shows that activations in t_0, τ_1, τ_2 and t_1 are used to interpolate activations in the backward pass.

3 Upper Bound on the Gradient Error Induced by Interpolated Activations

The proposed method excludes IVP that defines $z(t)$ from the adjoint IVP and uses approximation $\hat{z}(t)$ given by the barycentric Lagrange interpolation formula (7). Therefore, the dimension of the adjoint IVP is reduced, but the error in gradient $\frac{\partial L}{\partial \theta}$ appears since the activations are not exact. In this section, we present the upper bound on the gradient error norm and the factors that affect the

magnitude of this error. By the gradient error norm, we mean the norm of the difference between gradients computed with exact activations $\mathbf{z}(t)$ and interpolated ones $\tilde{\mathbf{z}}(t)$.

According to (4) we have to estimate the following error norm, where the 2-norm is used

$$E = \left\| \int_{t_0}^{t_1} \left[\tilde{\mathbf{a}}(t)^\top \frac{\partial f(\tilde{\mathbf{z}}(t), t, \boldsymbol{\theta})}{\partial \boldsymbol{\theta}} - \mathbf{a}(t)^\top \frac{\partial f(\mathbf{z}(t), t, \boldsymbol{\theta})}{\partial \boldsymbol{\theta}} \right] dt \right\|, \quad (9)$$

where $\tilde{\mathbf{a}}(t)$ and $\tilde{\mathbf{z}}(t)$ are adjoint variables and activations obtained with interpolation technique and $\mathbf{a}(t)$ and $\mathbf{z}(t)$ are exact ones. Now we derive the upper bound estimate of E and show what factors affect this upper bound. Introducing perturbations $\Delta \mathbf{z}(t)$ and $\Delta \mathbf{a}(t)$ such that $\tilde{\mathbf{a}}(t) = \mathbf{a}(t) + \Delta \mathbf{a}(t)$ and $\tilde{\mathbf{z}}(t) = \mathbf{z}(t) + \Delta \mathbf{z}(t)$ and using the first-order expansion of $\frac{\partial f}{\partial \boldsymbol{\theta}}$ at $\mathbf{z}(t)$ we can re-write terms from (9) with perturbed adjoint variables and activations as follows

$$\tilde{\mathbf{a}}(t)^\top \frac{\partial f(\tilde{\mathbf{z}}(t), t, \boldsymbol{\theta})}{\partial \boldsymbol{\theta}} = (\mathbf{a}(t) + \Delta \mathbf{a}(t))^\top \left(\frac{\partial f(\mathbf{z}(t), t, \boldsymbol{\theta})}{\partial \boldsymbol{\theta}} + \frac{\partial^2 f(\mathbf{z}(t), t, \boldsymbol{\theta})}{\partial \boldsymbol{\theta} \partial \mathbf{z}} \Delta \mathbf{z}(t) + \mathcal{O}(\|\Delta \mathbf{z}(t)\|^2) \right)$$

Substitution this equality in (9) and applying standard inequalities lead to the following upper bound

$$E \leq \int_{t_0}^{t_1} \|\mathbf{a}(t)\| \|\Delta \mathbf{z}(t)\| \left\| \frac{\partial^2 f(\mathbf{z}(t), t, \boldsymbol{\theta})}{\partial \boldsymbol{\theta} \partial \mathbf{z}} \right\| dt + \int_{t_0}^{t_1} \|\mathbf{a}(t)\| \left\| \frac{\partial f(\mathbf{z}(t), t, \boldsymbol{\theta})}{\partial \boldsymbol{\theta}} \right\| dt + \int_{t_0}^{t_1} \|\Delta \mathbf{a}(t)\| \|\Delta \mathbf{z}(t)\| \left\| \frac{\partial^2 f(\mathbf{z}(t), t, \boldsymbol{\theta})}{\partial \boldsymbol{\theta} \partial \mathbf{z}} \right\| dt + M_z \int_{t_0}^{t_1} (\|\mathbf{a}(t)\| + \|\Delta \mathbf{a}(t)\|) \|\Delta \mathbf{z}(t)\|^2 dt, \quad (10)$$

where $M_z > 0$ is a constant hidden in big-O notation. In order to estimate the error norm, we have to analyze bounds for all terms in (10). The norm of activations perturbation $\|\Delta \mathbf{z}(t)\|$ is bounded according to the upper bound on the interpolation error (8). At the same time, the gradient $\frac{\partial f(\mathbf{z}(t), t, \boldsymbol{\theta})}{\partial \boldsymbol{\theta}}$ and the second partial derivative $\frac{\partial^2 f(\mathbf{z}(t), t, \boldsymbol{\theta})}{\partial \boldsymbol{\theta} \partial \mathbf{z}}$ are not bounded a priori, so we need to consider them additionally. The remaining terms are $\|\mathbf{a}(t)\|$ and $\|\Delta \mathbf{a}(t)\|$ and to bound them we need the following Lemma [19].

Lemma 3.1 ([19], see Lemma 1)

Let $\mathbf{x}(t)$ be a solution of the following non-autonomous linear system

$$\begin{cases} \frac{d\mathbf{x}}{dt} = \mathbf{x}(t)^\top \mathbf{A}(t) + \mathbf{b}(t), \\ \mathbf{x}(t_0) = \mathbf{x}_0. \end{cases} \quad (11)$$

Then $\|\mathbf{x}(t)\| \leq \xi(t)$, where the scalar function ξ satisfies the IVP

$$\begin{cases} \frac{d\xi}{dt} = \mu[\mathbf{A}(t)]\xi + \|\mathbf{b}(t)\|, \\ \xi(t_0) = \|\mathbf{x}_0\|, \end{cases} \quad (12)$$

where $\mu[\mathbf{A}] \triangleq \lim_{h \rightarrow 0^+} \frac{\|\mathbf{I} + h\mathbf{A}\| - 1}{h}$ is a logarithmic norm of matrix \mathbf{A} [20].

If the 2-norm is used in definition of the logarithmic norm, then

$$\mu[\mathbf{A}] = \lambda_{\max} \left(\frac{\mathbf{A} + \mathbf{A}^\top}{2} \right),$$

where $\lambda_{\max}(\mathbf{A})$ is the maximum eigenvalue of a matrix \mathbf{A} .

In our case, IVP (11) is equivalent to IVP (3). Therefore, this lemma helps to estimate $\|\mathbf{a}(t)\|$. In particular, $\|\mathbf{a}(t)\| \leq \xi(t)$, where $\xi(t)$ is a solution of the following IVP:

$$\begin{cases} \frac{d\xi}{dt} = \mu[\mathbf{J}(t)]\xi, \\ \xi(t_1) = \left\| \frac{\partial L}{\partial \mathbf{z}_1} \right\|, \end{cases} \quad (13)$$

where $\mathbf{J}(t) \triangleq \frac{\partial f(\mathbf{z}(t), t, \boldsymbol{\theta})}{\partial \boldsymbol{\theta}}$. Hence, the upper bound on the adjoint variable norm is written with the solution of IVP (13):

$$\|\mathbf{a}(t)\| \leq \xi(t_1) \exp\left(\int_{t_1}^t \mu[\mathbf{J}(\tau)] d\tau\right). \quad (14)$$

The upper bound for $\|\Delta\mathbf{a}(t)\|$ can be also obtained with Lemma 3.1. To derive this upper bound, we compose an auxiliary IVP that defines a dynamic of $\Delta\mathbf{a}(t)$. Consider the following IVPs corresponding to exact and perturbed activations:

$$\begin{cases} \frac{d\mathbf{a}}{dt} = \mathbf{a}(t)^\top \frac{\partial f(\mathbf{z}(t), t, \boldsymbol{\theta})}{\partial \mathbf{z}} \\ \mathbf{a}(t_1) = \frac{\partial L}{\partial \mathbf{z}(t_1)} \end{cases} \quad \begin{cases} \frac{d\tilde{\mathbf{a}}}{dt} = \tilde{\mathbf{a}}(t)^\top \frac{\partial f(\tilde{\mathbf{z}}(t), t, \boldsymbol{\theta})}{\partial \mathbf{z}} \\ \tilde{\mathbf{a}}(t_1) = \frac{\partial L}{\partial \mathbf{z}(t_1)}. \end{cases} \quad (15)$$

Subtracting one IVP from the other, we get the IVP that defines dynamic of $\Delta\mathbf{a}(t) = \tilde{\mathbf{a}}(t) - \mathbf{a}(t)$:

$$\begin{cases} \frac{d\Delta\mathbf{a}(t)}{dt} = \Delta\mathbf{a}(t)^\top \mathbf{J}(t) + \tilde{\mathbf{a}}(t)(\tilde{\mathbf{J}}(t) - \mathbf{J}(t)) \\ \Delta\mathbf{a}(t_1) = \mathbf{0}. \end{cases} \quad (16)$$

Note that IVP (16) satisfies assumption in Lemma 3.1. Therefore, the following estimate holds

$$\|\Delta\mathbf{a}(t)\| \leq \xi(t), \quad (17)$$

where $\xi(t)$ is a solution of the following IVP:

$$\begin{cases} \frac{d\xi}{dt} = \mu[\mathbf{J}(t)]\xi + \|\tilde{\mathbf{a}}(t)(\tilde{\mathbf{J}}(t) - \mathbf{J}(t))\|, \\ \xi(t_1) = \mathbf{0}. \end{cases} \quad (18)$$

The solution of IVP (18) is given by the following formula

$$\xi(t) = \phi(t) \int_{t_1}^t \phi^{-1}(\tau) \|\tilde{\mathbf{a}}(\tau)(\tilde{\mathbf{J}}(\tau) - \mathbf{J}(\tau))\| d\tau, \quad (19)$$

where $\phi(t) = \exp\left(\int_{t_1}^t \mu[\mathbf{J}(\tau)] d\tau\right)$ is a fundamental solution of IVP (19). Thus, we get the upper bounds for all terms in the inequality (10).

Thus, we can list the factors that affect the accuracy of gradient approximation with interpolated activations. These factors are constants that bound $\frac{\partial f(\mathbf{z}(t), t, \boldsymbol{\theta})}{\partial \boldsymbol{\theta}}$ and $\frac{\partial^2 f(\mathbf{z}(t), t, \boldsymbol{\theta})}{\partial \boldsymbol{\theta} \partial \mathbf{z}}$ for $t \in [t_0, t_1]$ (10), logarithmic norm $\mu[\mathbf{J}(t)]$ (14), (17), (19), and smoothness of $\mathbf{J}(t)$ (19).

4 Numerical Experiments

In this section, firstly, we compare the proposed the IRDM with the RDM on the density estimation and variational inference tasks (for the RDM baselines, we use FFJORD [3] implementation). Secondly, we show the benefits of the IRDM on the CIFAR10 classification task (RDM implementation is similar to [1]). We demonstrate that during training, the IRMD requires less computational time to achieve convergence and a smaller number of evaluations of the right-hand side function comparing to the baselines. The source code of the proposed method can be found at GitHub¹.

Also, as the number of Chebyshev grid points N is an important hyperparameter in our method, we study how it affects the gain in considered tasks. Our method is implemented on top of `torchdiffeq`² package. The default ODE solver in our experiments is the DOPRI5. The values of optimized hyperparameters are in the supplementary materials. Mostly we follow the strategies from [3] and [9]. Every separate experiment is conducted on a single NVIDIA Tesla V100 GPU with 16Gb of memory [21]. We conducted all experiments with three different fixed random seeds and reported the mean value. Experiments were tracked using the ‘‘Weights & Biases’’ library [22].

¹<https://github.com/Daulbaev/IRDM>

²<https://github.com/rtqichen/torchdiffeq/>

Improvement in stability of gradient computations. We perform experiments on the reconstruction trajectory of the dynamical system that collapses in zero. As a result, we observe that the reverse dynamic method (RDM) and our method (IRDM) solve this problem with approximately the same accuracy. However, the RDM requires at least 10 times more right-hand side evaluations to solve adjoint IVP in every iteration than the IRDM. We use RDM implementation from the `torchdiffeq` package. Thus, in such a toy problem the IRDM and the RDM compute similar gradients, but the IRDM computes them much faster. To illustrate the stability of the IRDM, we show the plot of test loss vs. training time in density estimation problem, see Figure 3a.

How gradient approximation depends on the tolerance in adaptive solver and size of the Chebyshev grid. In Section 3, we provide theoretical bounds on the gradient approximation and list the main factors that affect it. However, tolerance in the adaptive solver and number of nodes in the Chebyshev grid can also significantly affect the quality of gradient approximation. To illustrate this influence empirically, we consider the toy dynamical system in 2D with the right-hand side Ay^3 and train neural ODE model to approximate trajectories of this dynamical system. We consider the range of tolerances in the DOPRI5 adaptive solver and the range of nodes quantities in the Chebyshev grid. The result of this experiment is presented in Figure 2. This plot shows that the smaller tolerance, the more accurate gradients approximation for all considered number of nodes in the Chebyshev grid. At the same time, the larger number of nodes leads to decreasing the approximation quality.

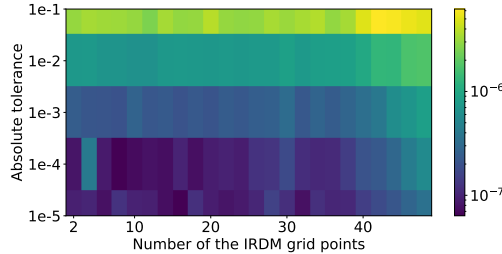


Figure 2: The dependence of the IRDM gradients error in ℓ_1 -norm with respect to the number of nodes in the Chebyshev grid and the tolerance of the DOPRI5 method. The output of the standard backpropagation performed for the DOPRI5 with $1e-7$ tolerance was used as a ground truth.

4.1 Density Estimation

The problem of density estimation is to reconstruct the probability density function using a set of given data points. We compared the proposed IRDM with the RDM (FFJORD³ [3] baseline) that exploits the reverse dynamic method to density estimation problem. We tested these methods on four toy datasets (`2spirals`, `pinwheel`, `moons` and `circles`) and tabular `miniboone` dataset [23]. This tabular dataset was used in our experiments since it is large enough and allows considered methods to converge for a reasonable time. According to [3] setting, we stopped the training process if, for the sequential 30 epochs, the test loss does not decrease. Therefore, we excluded test loss values given by the last 30 epochs from the plots. The model for `miniboone` was slightly different from the model from [3]; it includes 10 ODE blocks instead of 1. We used Adam optimizer [24] in all tests on the density estimation problem. For toy datasets, we used the following hyperparameters: learning rate equals 10^{-3} , the number of epochs was 10000, the batch size was 100, absolute and relative tolerances in the DOPRI5 solver were 10^{-5} and 10^{-5} .

Figure 3 shows that the test loss decreases more rapidly with our method than with the RDM. To make figures more clear, we plot convergence only for one value of N for every dataset. This value of N gives the best result among the tested values. Similar graphs for toy datasets can be found in Supplementary materials.

The number of nodes in the Chebyshev grid significantly affects the performance of the proposed method. If this number is small, then the interpolation accuracy is not enough, and the training takes a long time. If this number is large, then the computing of intermediate activations is too costly, and training is relatively slow. In supplementary materials, we provide graphs with empirical results on

³<https://github.com/rtqichen/ffjord>

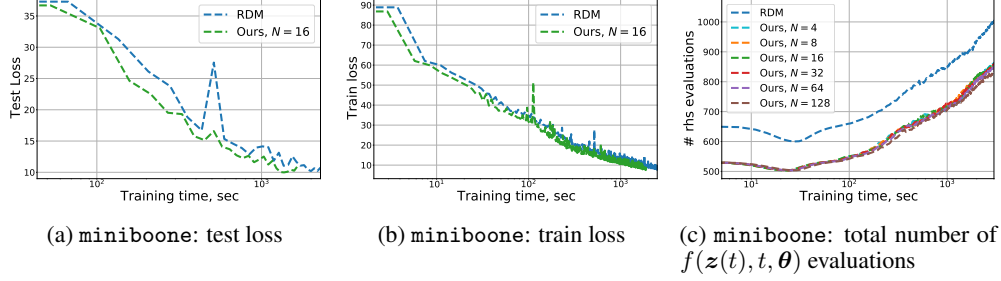


Figure 3: Comparison of the IRDM with the RDM (baseline from FFJORD) on density estimation problem for tabular dataset miniboone. The number of points in the Chebyshev grid N used in the IRDM is given in the legend.

how the number of points in the Chebyshev grid affects the convergence rate. On Figure 4, the total number of the right-hand side $f(z(t), t, \theta)$ evaluations per training iteration is shown.

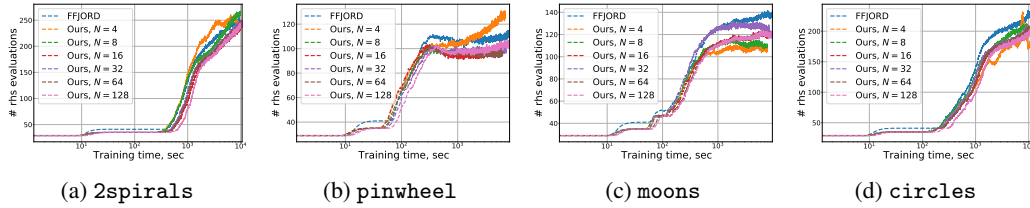


Figure 4: Total number of $f(z(t), t, \theta)$ evaluations for density estimation datasets.

4.2 Variational Autoencoder

We also compare the RDM (baselines from FFJORD) and the IRDM on the training variational autoencoder [25]. We use datasets caltech and freyfaces. The test negative ELBO loss and test bits per dim loss are reported for caltech and freyfaces datasets, respectively. Figure 5 illustrates a minor acceleration of convergence provided by the IRDM compared to the RDM. However, the IRDM gives the same final test loss with the same training time as the RDM. We suppose that the reason for such convergence degradation near the optimum is the same as for the density estimation models.

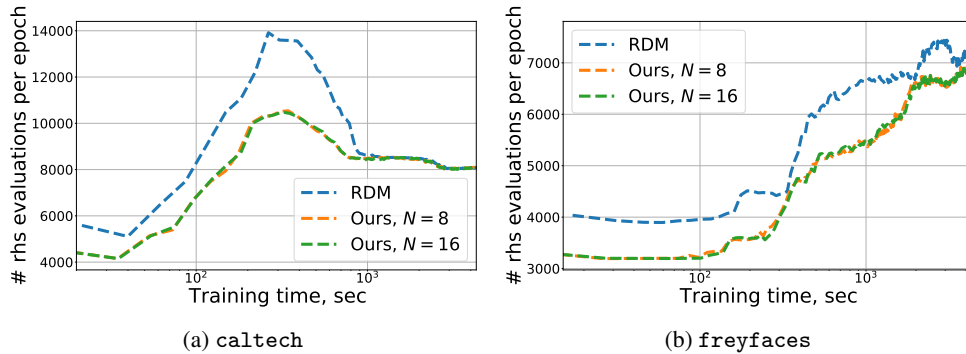
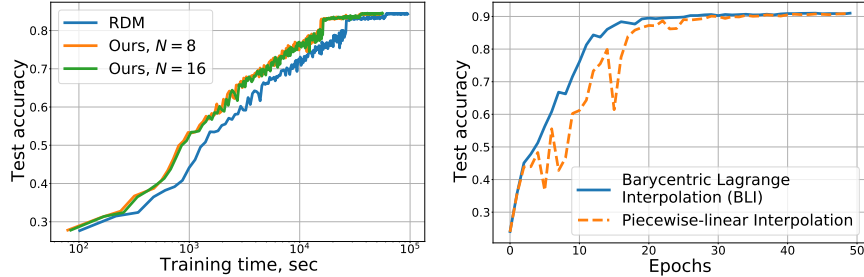


Figure 5: Comparison of the number of right-hand side evaluations for the IRDM and the RDM in training variational autoencoder.



(a) Comparison of the IRDM with the RDM in CIFAR10 classification task. IRDM even with $N = 8$ nodes trains faster than RDM. (b) Comparison of BLI and piecewise-linear interpolation used in the IRDM (8 nodes) in MNIST classification problem.

Figure 6: Experiments results in the image classification task. The reported values are averaged over three trained models corresponding to the considered tasks.

4.3 Classification

We test the proposed method on the classification problem with the CIFAR10 dataset. The model with a single convolution, a single ODE block, and a linear layer is considered. For this model, the IRDM with 16 points in the Chebyshev grid gives 0.867 test accuracy with the batch size 512 and tolerance $1e-3$ in the DOPRI5. We compare the IRDM with the RDM in terms of test loss versus training time. Figure 6a demonstrates that the IRDM gives higher test accuracy and requires less training time.

Another experiment is investigating whether other interpolation techniques can be used in the IRDM. We compare the Barycentric Lagrange Interpolation (BLI), which is a default method used in the IRDM, with the piecewise-linear interpolation. We perform 50 epochs in the MNIST classification problem with constant learning rate $1e-1$ and without data augmentation. Figure 6b confirms our choice of BLI since already after 40 epochs piecewise-linear interpolation provides less stable test accuracy behaviour.

5 Related Work

Neural ODEs [1] is a model inspired by the connection between neural networks and dynamical systems [26, 27, 28, 29]. Neural ODEs and its modifications were used for various different applications [3, 4, 30, 31, 32]. Nguyen et al. [33] emphasized the importance of using adaptive solvers and introduce a procedure to learn their tolerances. Quaglino et al. [34] proposed to use of spectral element methods, where the dynamics are expressed as a truncated series of Legendre polynomials. Similar ways of using interpolation in the adjoint method are implemented in SUNDIALS [35].

The proposed method relies on the ability of Runge-Kutta (RK) methods to evaluate the trajectory in intermediate points with Hermite polynomial interpolation. We use this feature of RK methods to evaluate activations in the Chebyshev grid points. The works by L. F. Shampine [36, 37] study the error induced by this approach to evaluate activations in intermediate points. In addition, the stiffness of ODE is an important concept [38, 39] for stable and fast training of neural ODEs.

6 Conclusion

We have presented the interpolated reverse dynamic method (IRDM) to improve the original reverse dynamic method (RDM) for training neural ODE models. The main idea of IRDM is to reduce the number of ODEs solved during the backward pass by using interpolated values $z(t)$ rather than ones found from equation (5). Thus, the total number of right-hand side evaluations during training and convergence time decreases compared to the original reverse dynamic method. We have empirically demonstrated this behavior on density estimation, variational inference, and classification tasks. Also, we have derived a theoretical upper bound on the error in computed gradients induced by the interpolation. The influence of the tolerance in adaptive ODE solver and the number of nodes in the Chebyshev grid is also studied numerically.

Broader Impact

We proposed a method for fast and stable Neural ODEs training. This method can be applied to any domain, where it is possible to use Neural ODEs. Since the IRDM reduces the time needed to train Neural ODEs, it has the potential to reduce the carbon footprint of building AI models.

Acknowledgement

Section 2 is supported by Ministry of Education and Science of the Russian Federation grant 14.756.31.0001. Section 3 was funded by RFBR, project number 19-29-09085 MK. Section 4 was funded by RFBR, project number 20-31-90127. High-performance computations presented in the paper were carried out on Skoltech HPC cluster Zhores [21].

References

- [1] Tian Qi Chen, Yulia Rubanova, Jesse Bettencourt, and David K Duvenaud. Neural ordinary differential equations. In *Advances in Neural Information Processing Systems*, pages 6571–6583, 2018.
- [2] Kaiming He, Xiangyu Zhang, Shaoqing Ren, and Jian Sun. Deep residual learning for image recognition. In *Proceedings of the IEEE conference on Computer Vision and Pattern Recognition*, pages 770–778, 2016.
- [3] Will Grathwohl, Ricky TQ Chen, Jesse Bettencourt, Ilya Sutskever, and David Duvenaud. Ffjord: Free-form continuous dynamics for scalable reversible generative models. *arXiv preprint arXiv:1810.01367*, 2018.
- [4] Yulia Rubanova, Tian Qi Chen, and David K Duvenaud. Latent Ordinary Differential Equations for Irregularly-Sampled Time Series. In *Advances in Neural Information Processing Systems*, pages 5321–5331, 2019.
- [5] LS Pontryagin, VG Boltyanskii, RV Gamkrelidze, and EF Mishchenko. *Mathematical Theory of Optimal Processes* {in Russian}, 1961.
- [6] Guri I Marchuk. *Adjoint Equations and Analysis of Complex Systems*, volume 295. Springer Science & Business Media, 2013.
- [7] Andreas Fichtner, H-P Bunge, and Heiner Igel. The adjoint method in seismology: I. theory. *Physics of the Earth and Planetary Interiors*, 157(1-2):86–104, 2006.
- [8] Matthew CG Hall. Application of adjoint sensitivity theory to an atmospheric general circulation model. *Journal of the Atmospheric Sciences*, 43(22):2644–2652, 1986.
- [9] Amir Gholami, Kurt Keutzer, and George Biros. ANODE: Unconditionally Accurate Memory-Efficient Gradients for Neural ODEs. *arXiv preprint arXiv:1902.10298*, 2019.
- [10] Radu Serban and Alan C Hindmarsh. CVODES: the sensitivity-enabled ODE solver in SUNDIALS. In *ASME 2005 international design engineering technical conferences and computers and information in engineering conference*, pages 257–269. American Society of Mechanical Engineers Digital Collection, 2005.
- [11] Jean-Paul Berrut and Lloyd N Trefethen. Barycentric Lagrange interpolation. *SIAM Review*, 46(3):501–517, 2004.
- [12] John R Dormand and Peter J Prince. A family of embedded Runge-Kutta formulae. *Journal of Computational and Applied Mathematics*, 6(1):19–26, 1980.
- [13] Michael B Giles and Niles A Pierce. An introduction to the adjoint approach to design. *Flow, Turbulence and Combustion*, 65(3-4):393–415, 2000.
- [14] R-E Plessix. A review of the adjoint-state method for computing the gradient of a functional with geophysical applications. *Geophysical Journal International*, 167(2):495–503, 2006.
- [15] Nicholas J Higham. The numerical stability of barycentric Lagrange interpolation. *IMA Journal of Numerical Analysis*, 24(4):547–556, 2004.
- [16] Bengt Fornberg. *A Practical Guide to Pseudospectral Methods*, volume 1. Cambridge university press, 1998.

- [17] Lloyd N Trefethen. *Spectral Methods in MATLAB*, volume 10. Siam, 2000.
- [18] Gerald B Folland. *Introduction to Partial Differential Equations*. Princeton university press, 1995.
- [19] Gustaf Söderlind and Robert MM Mattheij. Stability and asymptotic estimates in nonautonomous linear differential systems. *SIAM Journal on Mathematical Analysis*, 16(1):69–92, 1985.
- [20] Gustaf Söderlind. The logarithmic norm. History and modern theory. *BIT Numerical Mathematics*, 46(3):631–652, 2006.
- [21] Igor Zacharov, Rinat Arslanov, Maksim Gunin, Daniil Stefonishin, Andrey Bykov, Sergey Pavlov, Oleg Panarin, Anton Maliutin, Sergey Rykovanov, and Maxim Fedorov. “zhores”—petaflops supercomputer for data-driven modeling, machine learning and artificial intelligence installed in skolkovo institute of science and technology. *Open Engineering*, 9(1):512–520, 2019.
- [22] Lukas Biewald. Experiment Tracking with Weights and Biases, 2020. Software available from wandb.com.
- [23] Byron P Roe, Hai-Jun Yang, Ji Zhu, Yong Liu, Ion Stancu, and Gordon McGregor. Boosted decision trees as an alternative to artificial neural networks for particle identification. *Nuclear Instruments and Methods in Physics Research Section A: Accelerators, Spectrometers, Detectors and Associated Equipment*, 543(2-3):577–584, 2005.
- [24] Diederik P Kingma and Jimmy Ba. Adam: A method for stochastic optimization. *arXiv preprint arXiv:1412.6980*, 2014.
- [25] Diederik P Kingma and Max Welling. Stochastic gradient vb and the variational auto-encoder. In *Second International Conference on Learning Representations, ICLR*, volume 19, 2014.
- [26] Yiping Lu, Aoxiao Zhong, Quanzheng Li, and Bin Dong. Beyond finite layer neural networks: Bridging deep architectures and numerical differential equations. *arXiv preprint arXiv:1710.10121*, 2017.
- [27] Bo Chang, Lili Meng, Eldad Haber, Frederick Tung, and David Begert. Multi-level residual networks from dynamical systems view. *arXiv preprint arXiv:1710.10348*, 2017.
- [28] Lars Ruthotto and Eldad Haber. Deep neural networks motivated by partial differential equations. *Journal of Mathematical Imaging and Vision*, pages 1–13, 2018.
- [29] Christopher Rackauckas, Yingbo Ma, Julius Martensen, Collin Warner, Kirill Zubov, Rohit Supekar, Dominic Skinner, and Ali Ramadhan. Universal differential equations for scientific machine learning. *arXiv preprint arXiv:2001.04385*, 2020.
- [30] Julia Gusak, Larisa Markeeva, Talgat Daulbaev, Alexandr Katrutsa, Andrzej Cichocki, and Ivan Oseledets. Towards Understanding Normalization in Neural ODEs. *International Conference on Learning Representations (ICLR) Workshop on Integration of Deep Neural Models and Differential Equations*, 2020.
- [31] Tianjun Zhang, Zhewei Yao, Amir Gholami, Kurt Keutzer, Joseph Gonzalez, George Biros, and Michael Mahoney. ANODEV2: A Coupled Neural ODE Evolution Framework. *arXiv preprint arXiv:1906.04596*, 2019.
- [32] Emilien Dupont, Arnaud Doucet, and Yee Whye Teh. Augmented neural ODEs. *arXiv preprint arXiv:1904.01681*, 2019.
- [33] Tan M Nguyen, Animesh Garg, Richard G Baraniuk, and Anima Anandkumar. InfoCNF: An efficient conditional continuous normalizing flow with adaptive solvers. *arXiv preprint arXiv:1912.03978*, 2019.
- [34] Alessio Quaglino, Marco Gallieri, Jonathan Masci, and Jan Koutník. SNODE: Spectral Discretization of Neural ODEs for System Identification. *arXiv preprint arXiv:1906.07038*, 2019.
- [35] Alan C Hindmarsh, Radu Serban, Cody J Balos, David J Gardner, Carol S Woodward, and Daniel R Reynolds. User documentation for ida v5. 4.0 (sundials v5. 4.0). 2020.
- [36] Lawrence F Shampine. Interpolation for Runge–Kutta methods. *SIAM journal on Numerical Analysis*, 22(5):1014–1027, 1985.
- [37] Lawrence F Shampine. Some practical Runge–Kutta formulas. *Mathematics of Computation*, 46(173):135–150, 1986.

- [38] Gustaf Söderlind, Laurent Jay, and Manuel Calvo. Stiffness 1952–2012: Sixty years in search of a definition. *BIT Numerical Mathematics*, 55(2):531–558, 2015.
- [39] Gerhard Wanner and Ernst Hairer. *Solving Ordinary Differential Equations II*. Springer Berlin Heidelberg, 1996.

Appendix

A Number of Chebyshev grid points

In this section, we study how the quality of a model depends on the number of Chebyshev grid points. To demonstrate this dependence, we perform experiments with a range of N on toy two-dimensional datasets for the density estimation problem. Figures 7a and 7d show that if the number of nodes is too small, e.g., $N = 4$, the IRDM converges to the higher test loss. It means that the interpolation accuracy is not enough, and a larger number of points in the Chebyshev grid is needed. On the other hand, Figure 7 illustrates that if the number of nodes is too large, e.g., $N = 128$, the IRDM might be slower than the RDM. The reason is that a large number of nodes leads to the costly computations of the interpolated activations, see Equation (7) in the main text. Since the right-hand side function in the ODE block for toy datasets is easy to compute, the speedup effect is not much noticeable. However, the total number of the right-hand side function evaluations performed in IRDM is significantly smaller than in RDM, see Figure 8. Therefore, the more computationally expensive the right-hand side function is in the ODE block, the more significant gain one can get from using IRDM.

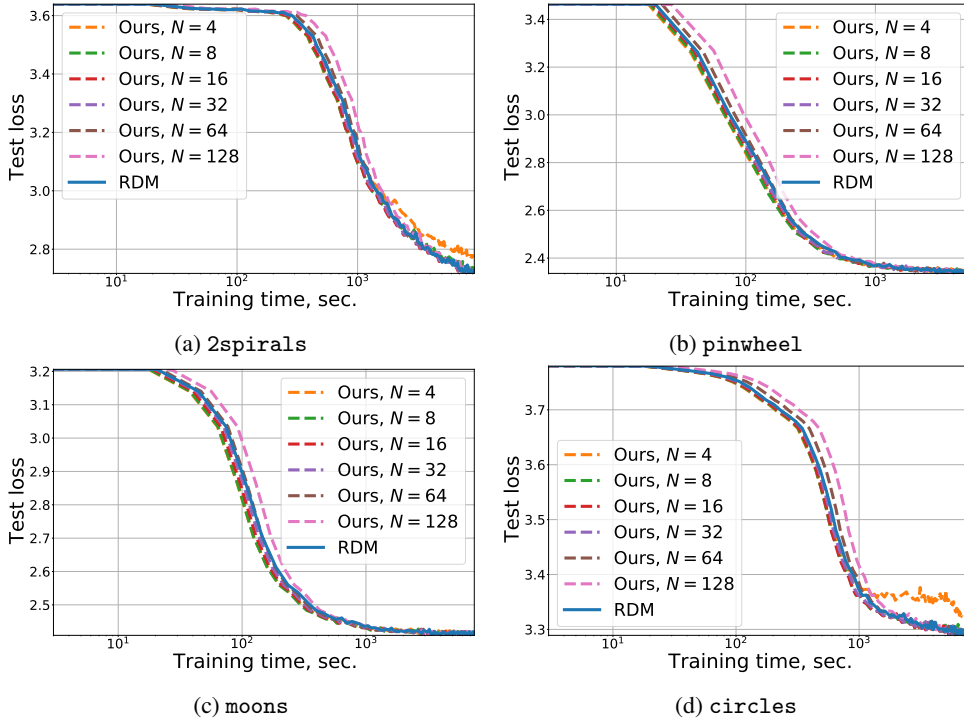


Figure 7: Comparison of IRDM (our method) and RDM on density estimation problem for toy datasets 2spirals, pinwheel, moons, and circles in terms of test loss versus wall-clock training time. Comparison results for every dataset are presented in the corresponding subplot. The number of points in Chebyshev grid N used in the IRDM is given in legend.

Table 1 shows the total time to perform 10000 training iterations for considered toy datasets. It can be seen that the IRDM with $N = 16$ nodes always outperforms the RDM.

B Experimental settings

To integrate ODE blocks in all experiments, we use the DOPRI5 ODE solver. We report mean test loss values and function evaluations values. These values are computed based on the ten runs with different fixed random seeds for toy datasets and three runs for other datasets.

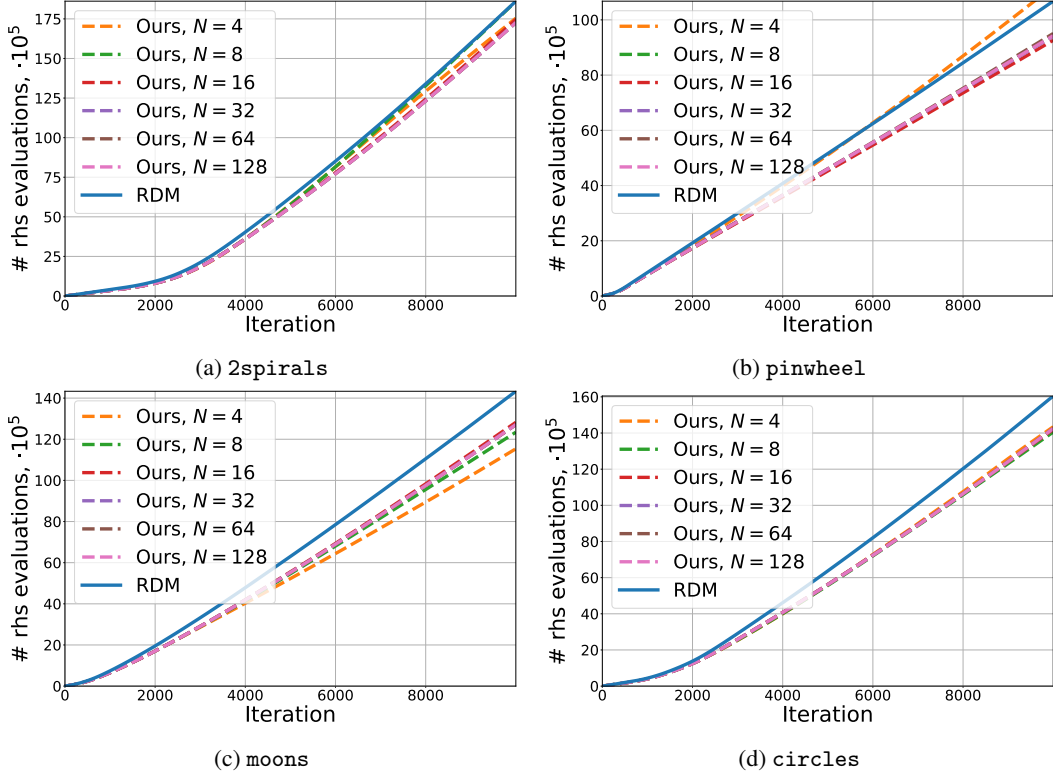


Figure 8: Comparison of IRDM (our method) and RDM on density estimation problem for toy datasets 2spirals, pinwheel, moons, and circles in terms of total number of the right-hand side evaluations versus number of iterations. Comparison results for every dataset are presented in the corresponding subplot. The number of points in Chebyshev grid N used in the IRDM is given in legend.

Table 1: Time (in seconds) to perform 10000 training iterations for toy datasets.

# nodes / dataset	RDM	4	8	16	32	64	128
pinwheel	5318	5389	4642	4750	4846	5152	5574
circles	7874	6927	6864	6842	7037	7578	8113
moons	7494	5618	6062	6471	6518	6720	7192
2spirals	9285	8998	9492	8938	8947	9267	9680

B.1 Classification

We test considered methods of neural ODE model training in the CIFAR10 classification task. We consider a model with a single ODE block, which consists of two convolutional layers with 64 input and output channels, ReLU activations, and weight normalizations. A convolutional layer with three input channels and 64 output channels, a batch normalization layer, and ReLU activation precede the ODE block. We use only random crops and random flips for data augmentation.

The training is performed by SGD with momentum 0.9. The weight decay is equal to $1e-5$; the learning rate is fixed and equal to $5e-3$, batch size is 100. Initial absolute and relative tolerances are set to $1e-5$. After the n^{th} 150 epoch, these tolerances are decreased by 10.

B.2 Density estimation

For the density estimation problem, we consider `miniboone` tabular dataset and four two-dimensional toy datasets. Data and preprocessing procedures are taken from <https://github.com/gpapamak/maf> and <https://github.com/rtqichen/ffjord>, respectively.

Instead of simple linear layers inside the ODE block, we use a so-called `concatsquash` linear layers, which are defined as follows

$$(\mathbf{W}\mathbf{z} + \mathbf{b}_1) \odot \sigma(t\mathbf{c} + \mathbf{b}_2) + t\mathbf{b}_3, \tag{20}$$

where \mathbf{z} are input activations, t stands for the time, \mathbf{W} , \mathbf{c} , \mathbf{b}_1 , \mathbf{b}_2 , \mathbf{b}_3 are trainable parameters, σ is a sigmoid activation, and \odot is an element-wise product.

For the `miniboone` dataset, we train a model with 10 ODE blocks and `softplus` nonlinearity. It is trained by Adam optimizer with a fixed learning rate equal to $1\text{e-}3$. The batch size is equal to 10000. Absolute and relative tolerances are set to $1\text{e-}8$ and $1\text{e-}7$, respectively. The training terminates if test loss does not decrease during 30 sequential epochs.

In experiments with toy datasets, a model with a single ODE block is used. This ODE block consists of three `concatsquash` linear layers of size 2×64 , 64×64 , and 64×2 . To train the Neural ODEs model, SGD with momentum 0.9 and fixed learning rate $1\text{e-}3$ is used. Absolute and relative tolerances are set to $1\text{e-}5$. The number of iterations in the training procedure is 10000, and 100 samples compose mini-batch.

B.3 VAE

For VAE experiments, we choose two datasets: `caltech` and `freyfaces`. Both datasets can be found in <https://github.com/riannevdberg/sylvester-flows>. All the experimental settings are exactly the same as in the FFJORD paper. The only difference is that IRDM is used to train models instead of RDM.